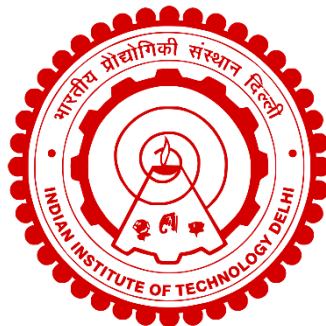


**PERFORMANCE ANALYSIS AND OPTIMIZATION OF
MINERAL SILICATE FILLED LOW METALLIC
COMPOSITE FRICTION MATERIALS**

DEBARGHYA SAHA



**DEPARTMENT OF MATERIALS SCIENCE AND ENGINEERING
INDIAN INSTITUTE OF TECHNOLOGY DELHI
OCTOBER 2022**

©Indian Institute of Technology Delhi (IITD), New Delhi, 2022

**PERFORMANCE ANALYSIS AND OPTIMIZATION OF
MINERAL SILICATE FILLED LOW METALLIC
COMPOSITE FRICTION MATERIALS**

by

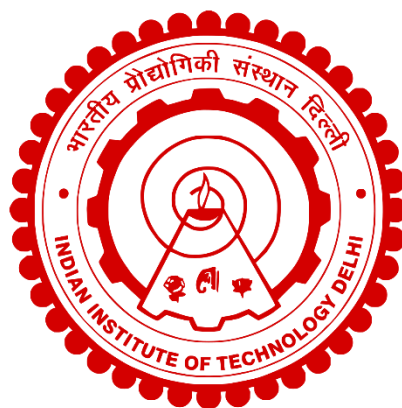
DEBARGHYA SAHA

Department of Materials Science and Engineering

Submitted

in fulfilment of the requirements of the degree of Doctor of Philosophy

to the



INDIAN INSTITUTE OF TECHNOLOGY DELHI

OCTOBER 2022

Dedicated to my family

CERTIFICATE

This is to certify that the thesis entitled, “**Performance Analysis and Optimization of Mineral Silicate Filled Low Metallic Composite Friction Materials**” being submitted by Mr. Debarghya Saha to Indian Institute of Technology Delhi for the award of degree of Doctor of Philosophy is a record of bonafied research work carried out by him. Mr. Saha has worked under my guidance and supervision and has fulfilled the requirements for the submission of this thesis, which to my knowledge has reached the requisite standard. The results contained in this thesis are original and have not been submitted, in part or full, to any other University or Institute for the award of any other degree or diploma.

Professor Bhabani K. Satapathy

Department of Materials Science & Engineering

Indian Institute of Technology Delhi

Hauz Khas, New Delhi- 110016

ACKNOWLEDGEMENTS

Foremost, I would like to thank my supervisor Prof. Bhabani K. Satapathy, for his continuous support, guidance, and motivation for my Ph.D. dissertation. It was a truly enlightening journey that helped me understand and explore this exciting scientific research area and address the problems. His involvement in my research was inspirational and always provided a new horizon toward my perspective while addressing any issue. On several occasions, his pretension of being hard pushed me to work harder and extended my knowledge in various science and technology domains. This journey with him will always remain memorable and cherishable for me during my entire life.

I am thankful to Prof. A.K. Ghosh, Prof. Leena Nebhani, and Prof. Pulak M Pandey, for their constructive comments, suggestions, and encouragements during my semester evaluation. I acknowledge Prof. J Jacob, Prof. S Saha, Prof. B P Tripathi, Prof. Shib Shankar Banerjee and other faculty members in DMSE for their support and encouragement.

I would like to take this opportunity to express my gratitude to Mr. Etheshamul Islam, Mr. Ashok Kapoor, Mr. Surinder Sharma, Mr. Ashish Sharma, Mr. Gajraj Singh, Mr. Brijesh Kumar, Mr. Gyanendra Kr. Yadav, Mr. Subhash Chand, Mr. Jitendra Kumar, Mrs. Shalini Arora, and Mr. Amit Kumar for their technical support to implement my research. I appreciate the members of our research group Dr. Sucharita Shetty, Dr. Deepika Sharma, Mr. Saroj K. Samantaray, Mr. Harshal Peshne, Mr. Vikram Thakur, Ms. Krishna P. Das and Ms. Pratibha for their help and support. I also thank all the students of the Department of Materials Science and Engineering for their continuous encouragement. Finally, I would like to thank my parents and family members for their unconditional support in this journey.

I am very grateful to the Ministry of Education for providing a Ph.D. research fellowship.

ABSTRACT

Phenolic resin-based short fiber reinforced and filled heterogeneous material system as composite friction materials are the part of the vehicle's braking system that is responsible for the overall safety of the passenger. Pertaining to the microplastic and particulate matter emission due to the presence of synthetic and metallic ingredients in the form of brake wear debris the recent requirement is to design sustainable bio-resourced, naturally derived ingredient-based friction composites. Therefore, designing sustainable and commercially viable friction materials for braking applications without compromising the thermal stability and frictional-fade resistance remains a challenge especially in formulations with a substantial amount of thermally degradable components. To address the above issue structurally dissimilar clay type silicates, halloysite (tubular), montmorillonite (platy), and wollastonite (acicular)-based compression-molded low metallic hybrid friction composites were fabricated with and without magnesium oxide (MgO) followed by their structural, mechanical, thermal, thermo-mechanical, and tribological performance evaluation. Wollastonite type clay-based friction composite showed maximum CoF (~ 0.48) during the fade-recovery test (as per SAEJ661a testing protocol), whereas the montmorillonite type clay silicate exhibited maximum wear resistance ($\sim 8.3\%$) with a greater extent of friction stabilization as supported by I_D/I_G data from Raman spectra. The combination of halloysite–MgO in the friction composite led to minimum fade ($\sim 2.2\%$), whereas that of wollastonite–MgO showed a maximum friction coefficient (~ 0.47) with enhanced rotor friendliness as indicated from optical surface profilometry. The friction fade-recovery behaviour was correlated with sliding induced interfacial contact dynamics showing three distinct phases i.e., uniform tribo-film formation, brittle tribo-layer, and subsurface exposer-third body abrasion. During velocity dependent friction response scanning electron microscopy of the contact patches suggested breakage of contact plateaus in the composites with halloysite, whereas relatively small contact patches

were developed in montmorillonite-based friction composites. The presence of wollastonite in the composites leads to the ploughing effect during sliding. The intensity of creep groan remained controlled by the shear strength of the interfacial junction involving asperity contact/welding whereas dynamic groan remains predominated by the stiffness of the composites. The optimal tuning of friction oscillation to reduce braking-induced noise and vibration propensity has been achieved by montmorillonite clay with platelet-type morphology. Where the extent of Fe- content in wear debris close to ~80% on the composite surface led to an optimal level of friction oscillation amplitude (A_{amp}). The friction response during cyclic loading showed montmorillonite-based composites characterized by maximum hysteresis loss due to the difference between μ -level during loading and unloading in presence of MgO as an abrasive. Wollastonite with the relatively minimum area to volume ratio showed inefficient reinforcement in the tribo-film thus debris formation and subsequent third body abrasion leading to undulating μ -level. Similarly, the composites with circular and transverse cracks over the surface demonstrated fatigue wear-mechanism. The non-linear regression-based optimization showed minimum volumetric wear (< 7 %) of the fabricated friction composites. The tribological performance attributes were governed by the relative abrasiveness of the clay types and reversible plateau dynamics of the worn surfaces. The gradient descent learning algorithm based-artificial neural network (GD-ANN) with optimally tuned network architecture predicted ($R^2 \sim 97\%$) both the tribological performance attributes (coefficient of friction and specific wear rate) of the natural silicate-filled friction composites more accurately as compared to the conventional regression analysis. The performance attributes were governed by the compressive stiffness of the friction composites, hardness, thermal stability, and morphological aspects of the clay-type silicates, and their induced contact dynamics as evident from scanning electron microscopy–energy-dispersive X-ray spectroscopy (SEM–EDX) studies.

सार

मिश्रित घर्षण सामग्री के रूप में फेनोलिक राल-आधारित शॉर्ट फाइबर प्रबलित और भरी हुई विषम सामग्री प्रणाली वाहन के ब्रेकिंग सिस्टम का हिस्सा है जो यात्री की समग्र सुरक्षा के लिए जिम्मेदार है। ब्रेक वियर मलबे के रूप में सिंथेटिक और धात्विक अवयवों की उपस्थिति के कारण माइक्रोप्लास्टिक और पार्टिकुलेट मैटर उत्सर्जन से संबंधित, हाल की आवश्यकता टिकाऊ जैव-संसाधन, स्वाभाविक रूप से व्युत्पन्न संघटक-आधारित घर्षण कंपोजिट को डिजाइन करने की है। इसलिए, थर्मल स्थिरता और घर्षण-फीका प्रतिरोध से समझौता किए बिना ब्रेकिंग अनुप्रयोगों के लिए टिकाऊ और व्यावसायिक रूप से व्यवहार्य घर्षण सामग्री को डिजाइन करना विशेष रूप से थर्मली डिग्रेडेबल घटकों की पर्याप्त मात्रा के साथ फॉर्मूलेशन में एक चुनौती बनी हुई है। उपरोक्त मुद्दे को संरचनात्मक रूप से भिन्न मिट्टी के प्रकार के सिलिकेट, हेलोसाइट (ट्यूबलर), मॉन्टमोरिलोनाइट (प्लेटी), और वोलास्टोनाइट (एसिकुलर) आधारित संपीडन-मोल्ड कम धातु हाइब्रिड घर्षण कंपोजिट को मैग्नीशियम ऑक्साइड (एमजीओ) के साथ और बिना गढ़ा गया था।, मैकेनिकल, थर्मल, थर्मो-मैकेनिकल और ट्राइबोलॉजिकल परफॉर्मंस मूल्यांकन। फेड-रिकवरी टेस्ट (एसईजे 661 ए परीक्षण प्रोटोकॉल के अनुसार) के दौरान वोलास्टोनाइट प्रकार की मिट्टी-आधारित घर्षण समग्र ने अधिकतम सीओएफ (~ 0.48) दिखाया, जबकि मॉन्टमोरिलोनाइट प्रकार के क्ले सिलिकेट ने घर्षण स्थिरीकरण की अधिक सीमा के साथ अधिकतम पहनने के प्रतिरोध (~ 8.3%) का प्रदर्शन किया। जैसा कि रमन स्पेक्ट्रा से आईडी/आईजी डेटा द्वारा समर्थित है। घर्षण सम्मिश्र में हेलोसाइट-एमजीओ के संयोजन से न्यूनतम फीका (~2.2%) हो गया, जबकि वोलास्टोनाइट-एमजीओ ने अधिकतम घर्षण गुणांक (~0.47) को बढ़ाया रोटार मित्रता के साथ दिखाया जैसा कि ऑप्टिकल सतह प्रोफिलोमेट्री से संकेत मिलता है। घर्षण फीका-पुनर्प्राप्ति व्यवहार को तीन अलग-अलग चरणों यानी एक समान ट्राइबो-फिल्म निर्माण, भंगुर ट्राइबो-लेयर और उपसतह एक्सपोजर-थर्ड बॉडी घर्षण दिखाते हुए स्लाइडिंग प्रेरित इंटरफेसियल कॉन्टैक्ट डायनेमिक्स के साथ सहसंबद्ध किया गया था। वेग पर निर्भर घर्षण प्रतिक्रिया के दौरान संपर्क पैच के स्कैनिंग इलेक्ट्रॉन माइक्रोस्कोपी ने हेलोसाइट के साथ कंपोजिट

में संपर्क पठारों के टूटने का सुझाव दिया, जबकि अपेक्षाकृत छोटे संपर्क पैच मॉन्टमोरिलोनाइट-आधारित घर्षण कंपोजिट में विकसित किए गए थे। कंपोजिट में वोलास्टोनाइट की उपस्थिति से फिसलने के दौरान जुताई का प्रभाव पड़ता है। रेंगने वाले कराह की तीव्रता को इंटरफेसियल जंक्शन की कतरनी शक्ति द्वारा नियंत्रित किया जाता है जिसमें एस्पिरिटी संपर्क / वेल्डिंग शामिल होता है जबकि गतिशील कराह कंपोजिट की कठोरता से प्रबल होती है। ब्रेकिंग-प्रेरित शोर और कंपन प्रवृत्ति को कम करने के लिए घर्षण दोलन का इष्टतम ट्यूनिंग प्लेटलेट-प्रकार आकारिकी के साथ मॉन्टमोरिलोनाइट क्ले द्वारा प्राप्त किया गया है। जहां मिश्रित सतह पर 80% के करीब पहनने वाले मलबे में Fe- सामग्री की सीमा घर्षण दोलन आयाम (Aamp) का एक इष्टतम स्तर है। चक्रीय लोडिंग के दौरान घर्षण प्रतिक्रिया ने मॉन्टमोरिलोनाइट-आधारित कंपोजिट को अधिकतम हिस्टैरिसिस नुकसान की विशेषता दिखायी, जो कि एमजीओ की उपस्थिति में एक अपघर्षक के रूप में लोडिंग और अनलोडिंग के दौरान μ -स्तर के बीच अंतर के कारण होता है। वॉल्यूम अनुपात के अपेक्षाकृत न्यूनतम क्षेत्र के साथ वोलास्टोनाइट ने ट्राइबो-फिल्म में अक्षम सुदृढीकरण दिखाया, इस प्रकार मलबे का निर्माण और बाद में तीसरे शरीर के घर्षण के कारण μ -स्तर को कम करना पड़ा। इसी तरह, सतह पर वृत्ताकार और अनुप्रस्थ दरारें वाले कंपोजिट ने थकान पहनने-तंत्र का प्रदर्शन किया। गैर-रेखीय प्रतिगमन-आधारित अनुकूलन ने गढ़े हुए घर्षण कंपोजिट के न्यूनतम वॉल्यूमेट्रिक वियर (<7%) को दिखाया। आदिवासी प्रदर्शन विशेषताओं को मिट्टी के प्रकार के सापेक्ष घर्षण और पहना सतहों के प्रतिवर्ती पठार की गतिशीलता द्वारा नियंत्रित किया गया था। प्राकृतिक सिलिकेट से भरे घर्षण कंपोजिट के आदिवासी प्रदर्शन विशेषताओं (घर्षण और विशिष्ट पहनने की दर का गुणांक) दोनों की भविष्यवाणी की गई नेटवर्क आर्किटेक्चर (R2 97%) के साथ ग्रेडिएंट डिसेंट लर्निंग एल्गोरिदम आधारित-कृत्रिम तंत्रिका नेटवर्क (GD-ANN) अधिक पारंपरिक प्रतिगमन विश्लेषण की तुलना में सटीक रूप से। प्रदर्शन विशेषताओं को घर्षण कंपोजिट, कठोरता, थर्मल स्थिरता, और मिट्टी के प्रकार के सिलिकेट्स के रूपात्मक पहलुओं और उनके प्रेरित संपर्क गतिशीलता की संपीड़ित कठोरता द्वारा नियंत्रित किया गया

था, जैसा कि इलेक्ट्रॉन माइक्रोस्कोपी-ऊर्जा-फैलाने वाले एक्स-रे स्पेक्ट्रोस्कोपी (एसईएम) को स्कैन करने से स्पष्ट है। -EDX) अध्ययन।

TABLE OF CONTENTS

CERTIFICATE.....	i
ACKNOWLEDGEMENTS.....	iii
ABSTRACT.....	iv
संर.....	vi
LIST OF FIGURES	xiv
LIST OF TABLES.....	xxi
LIST OF ABBREVIATIONS.....	xxiii
Chapter 1 : Introduction, literature review, motivation, and objectives	1
1.1. Preamble	2
1.2. Introduction.....	3
1.3. Historical evolution of friction composites.....	6
1.4. Braking induced contact dynamics dependent particulate matter emission from friction composites.....	8
1.4.1. Third body abrasion.....	9
1.4.2. Primary contact plateau	10
1.4.3. Secondary contact plateau	10
1.5. Environmental impact of friction composites.....	12
1.5.1. Generation of microplastics from braking dynamics	14
1.5.1.1. Assessment of microplastic deposition on soils.....	15
1.5.1.2. Deposition and transportation of microplastics in water.....	16
1.5.1.3. Assessment of microplastics as airborne particles and hazards thereof.....	18
1.5.2. Wear resistant brake friction composites	19
1.5.3. Asbestos-free brake friction composites	24
1.5.4. Copper-free brake friction composites.....	25
1.5.5. Antimony free brake friction composites.....	29
1.5.6. Metal-free brake friction composites	30
1.6. Prospects of green ingredients in friction composites	31
1.6.1. Prospects of binder modification for toxicity-reduction and bio-based resins in friction composites	32
1.6.2. Prospects of bio-fibers and bio-processing of fibers in friction composites	34
1.6.3. Role of functional additives in friction composites	38
1.6.3.1. Lubricants	38
1.6.3.2. Abrasives	40
1.6.2.3. Space fillers	41
1.7. Life cycle assessment.....	44
1.8. Strength-weakness-opportunity-threat (SWOT) analysis on the compositional aspects of the brake friction composites.....	47

1.9. Strategy assessment	50
1.10. Modelling and tribological performance prediction of friction composites	54
1.11. Wear Prediction:	56
1.12. Artificial neural network.....	56
1.13. Challenges and future perspective	58
1.14. Concluding remarks	59
1.15. Key questions.....	60
1.16. Motivation of the work	61
1.17. Research objective	62
1.18. Format of the thesis.....	62
Chapter 2 : Experimental: Materials and methodology	66
2.1. Composite designation and fabrication.....	67
2.2. Physical, mechanical and surface characterizations	69
2.3. Tribological performance evaluation	69
2.3.1. Friction fade-recovery behaviour.....	69
2.3.2. Instantaneous braking performance evaluation.....	72
2.3.3. Stick-slip Analysis	72
2.3.4. Friction oscillation evaluation	73
2.3.4.1. Experimental Design	74
2.3.5. Friction hysteresis evaluation under cyclic load	76
2.3.6. Load, speed, and temperature sensitivity analysis	76
2.4. Characterization	78
2.4.1. Thermal, mechanical, and thermo-mechanical properties	78
2.4.2. Morphological characterizations.....	79
2.4.3. Modelling with gradient descent training algorithm-based artificial neural network (GD-ANN).....	80
Chapter 3 : Compositional and parametric influence on friction oscillation amplitude of clay type silicate-based friction composites	84
3A. Friction fade-recovery performance and interfacial braking dynamics of the clay type silicate-based phenolic composites	86
3A.1. Introduction.....	86
3A.2. Thermo-physical, structural, and morphological characterization of the clay minerals	86
3A.3. Physical, mechanical and surface characterization	90
3A.4. Loss modulus and glass transition behaviour of the friction composites	90
3A.5. Friction evolution characteristics of the composites.....	91
3A.6. Comparative friction performance assessment	95
3A.7. Braking induced interfacial contact dynamics	98
3A.8. Friction fluctuation and Stability(α) and variability (γ) coefficient.....	99
3A.9. Wear behaviour analysis	101

3A.10. Worn surface morphology and wear debris analysis	102
3A.11. Summary	108
3B. Combinatorial effects of clay type silicate and MgO on friction braking performance of hybrid phenolic composites	110
3B.1. Introduction	110
3B.2. Thermo-mechanical and morphological characteristic of the clay silicates	111
3B.3. Dynamic mechanical analysis of the fabricated composites	113
3B.4. Friction evolution characteristic	114
3B.5. Comparative friction performance assessment	117
3B.6. Friction fluctuation and coefficient of stability (α) and variability (γ)	120
3B.7. Wear behaviour analysis	122
3B.8. Worn surface morphology analysis	123
3B.9. Friction performance under the instantaneous braking condition	127
3B.10. Summary	129
Chapter 4 : Compositional and parametric influence on friction oscillation amplitude of clay type silicate-based friction composites	131
4A. Influence of various types of clays on velocity dependence of friction composites	133
4A.1. Introduction	133
4A.2. Dynamic mechanical analysis	133
4A.3. Stick-slip analysis	136
4A.3.2. Stick-slip behaviour	139
4A.3.3. Friction attribute triggering creep groan	142
4A.4. Worn surface morphology	143
4A.4.1. Scanning electron microscopic (SEM) analysis	143
4A.4.2. Energy dispersive analysis of X-Rays (EDAX)	148
4A.5. Analytical model of stick slip behaviour	150
4A.6. Parametric influence on stick-slip amplitude	155
4A.7. Summary	157
4B. Tuning of friction oscillation amplitude in halloysite, montmorillonite, and wollastonite filled friction composites: load, speed, and temperature sensitivity	160
4B.1. Introduction	160
4B.2. Friction Performance Evaluation	160
4B.3. Taguchi analysis for friction oscillation amplitude (A_{amp})	163
4B.4. Confirmation Experiment	165
4B.5. Worn Surface Morphology	167
4B.5.1. Scanning Electron Microscopy (SEM) Analysis	167
4B.5.2. Role of clay morphology in friction oscillation	169
4B.5.3. Surface Roughness Analysis	170

4B.5.4. Energy Dispersive X-ray (EDX) Analysis	172
4B.6. Analysis of friction oscillation through regression model	176
4B.7. Performance hierarchy of the friction composites	178
4B.7.1. Steps Involved in TOPSIS	179
4B.7.2. Steps Involved in TOPKOR.....	180
4B.7.3. Analysis of Preference Order	181
4B.8. Summary	182
Chapter 5 : Friction hysteresis and subsequent wear mechanism of clay-based phenolic composites under cyclic load	184
5. Friction hysteresis and subsequent wear mechanism of clay-based phenolic composites under cyclic load	186
5.1. Introduction.....	186
5.2. Friction hysteresis	186
5.2.1. General Characteristics of the friction hysteresis curve.....	186
5.2.2. Contribution of clay minerals in friction hysteresis.....	188
5.3. Worn surface morphology and wear behaviour of the composites.....	191
5.3.1. SEM micrographs of the worn surface	191
5.3.2. Wear behavior of the composites.....	193
5.3.3. Worn surface roughness after hysteresis cycle	194
5.4. Summary.....	197
Chapter 6 : Performance sensitivity analysis, performance prediction, and targeted material design for the clay-based friction composites.....	199
6A. Targeted material design for clay-based friction composite with non-linear regression approach	201
6A.1. Introduction.....	201
6A.2. Tribological performance attribute and non-linear regression optimization	201
6A.2.1. Design ideology 1	206
6A.2.2. Design ideology 2	206
6A.3. Performance validation	209
6A.3.1. Comparative friction response of the CFMs	210
6A.3.2. Friction performance of the composites.....	214
6A.3.3. Friction-fade and friction recovery performance	216
6A.3.4. Wear behavior and worn surface morphology	218
6A.4. Summary	220
6B. Performance sensitivity analysis of natural mineral silicates filled friction composites using GD – ANN approach.	222
6B.1. Introduction	222
6B.2. Compressive strength analysis	222
6B.3. Dynamic mechanical analysis	224
6B.3.1. Viscoelastic storage modulus	224

6B.3.2. Energy dissipation/ loss modulus/ damping properties	225
6B.4. Effect of braking load on the coefficient of friction and wear (load sensitivity)	227
6B.5. Effect of sliding speed on the coefficient of friction and wear (speed sensitivity)	228
6B.6. Effect of temperature on the coefficient of friction and wear (temperature sensitivity)	230
6B.7. Worn surface morphology analysis	233
6B.8. Tribo-layer characterization	235
6B.9. Tribological performance prediction	239
6B.9.1. Regression analysis	239
6B.9.2. GD-ANN model	243
6B.10. Summary	248
Chapter 7 : Conclusion and future outlook	249
7.1. Conclusion	250
7.2. Future scope	253
Bibliography	254
List of Publications and Biography	279
List of publications	280
Biography:.....	282

LIST OF FIGURES

Figure 1.1. (a) components of a typical automotive brake pad (b) functional properties of brake friction composites, (c and c') semi-metallic brake lining, (d and d') organic brake pad, and (e and e') ceramic brake pad [16]	5
Figure 1.2. Historical evolution of brake friction composites	7
Figure 1.3. Schematic representation of (a) sliding induced contact dynamics (i) enhanced topographical contrast, and (ii) enhanced compositional contrast [38], (b) primary plateau and secondary plateau [38]; (c) Secondary contact plateau of type I and type II [11].	12
Figure 1.4. Environmental impact of brake friction composites (a) non-exhaust vehicular emission in New Delhi, India [51] (b) dynamometer testing of brake wear particles under urban driving cycles [52] (c) Particle mass concentration (of PM ₁₀ and PM _{2.5}) with respect to time and speed [53] (d) Time series data of the sources of PM emission in Delhi (i) Evaporation of volatile organic compounds (ii) PM ₁₀ from the road dust (iii) PM ₁₀ emission from tyre wear (iv) PM ₁₀ emission from brake wear [54].	13
Figure 1.5. BWDs at two magnifications (a-b) with scale bar 10 μm, (c-d) with scale bar 2 μm [67]; Elemental mapping of the BWDs from (a) NAO brake pad and (b) low metallic brake pad [95].	20
Figure 1.6. Cu-free brake friction composites (a) US regulations on the various components of brake friction composites [132] (b) DNA damage score of Cu associated microplastics on <i>P. lineatus</i> fish with water (CTR), 20 μg MP L ⁻¹ (MP), 10 μg Cu L ⁻¹ (Cu) or 20 μg MP L ⁻¹ plus 10 μg Cu L ⁻¹ (MP + Cu) for 24 h and 96 h on i. erythrocytes ii. liver and iii. gills iv. different classes of comets deciding the DNA damage score [124]; (c) time series data of particle number concentration and PM ₁₀ during pin on disc study of brake friction composites with and without Cu [126]; SEM images of friction dust (d) based on CNSL (e) Cardanol (f) boron modified (g) boron-Graphite modified [130].	27
Figure 1.7. Types of plant fibers used in designing green brake friction composites [181].	35
Figure 1.8. Micrographs of various naturally derived and additives based on industrial waste for sustainability (a) natural graphite [137], (b) red mud [224], (c) mullite [236], (d) periwinkle shell powder [226], (e) ulexite [237], (f) white arc shell powder [228], (g) BaSO ₄ [214], (h) CaCO ₃ [214], and (i) fly-ash [238].	42
Figure 1.9. SWOT analysis of the conventional NAO type semi-metallic and low metallic brake friction composites, alongside the recently explored metal-free, bio-derived/ naturally	

occurring ingredients-based brake friction composites based on reported data and performance attributes [202, 204].	48
Figure 1.10. Compositional variation of brake friction composites (with bio-based, hydrocarbon, and metallic ingredients), and its subsequent impact on microplastics generation/ PM emission as air, soil and water contaminants.	50
Figure 1.11. The compositional influence on functional attributes of the brake friction composites as indicated in the composition-performance relational matrix (a) semi metallic/ low-metallic brake friction composites (b) bio-resourced naturally ingredients-based brake friction composites.	52
Figure 1.12. MCA modelling setup steel substrate marked with grey, violet color represents graphite, and SiC represented with bright magenta [265]	55
Figure 2.1. Schematic representation of chase type friction tester, and friction interface (inset) during the test.	70
Figure 2.2. Step-wise collection of the developed tribo-layer after load, speed, and temperature sensitivity Analysis.	80
Figure 2.3. The architecture of the neural network with input and output parameters.	83
Figure 3A.1. The morphology of (a) halloysite, (b) montmorillonite, and (c) wollastonite type clay silicates; (d) thermogravimetric plot of clay-type silicates.	88
Figure 3A.2 The XRD spectra and hydrodynamic radii of, (a) Halloysite, (b) Montmorillonite, and (c) Wollastonite type clay silicate in pristine form and after 1000 °C heat treatment.	89
Figure 3A.3. The temperature-dependent loss modulus of clay-type silicate-based friction composites.	91
Figure 3A.4. Friction evolution characteristics and load-displacement behaviour of (a and a') C0, (b and b') CH, (c and c') CM, (d and d') CW friction composites.	94
Figure 3A.5. Comparative friction performance of the clay type silicate-based friction composites during (a) first fade run (FFR), (b) first recovery run (FRR), (c) second fade run (SFR), and (d) second recovery run (SRR).	96
Figure 3A.6. Schematic representation of the Braking induced interfacial contact dynamics	99
Figure 3A.7. Friction performance attributes of the clay type silicate-based composites (a) μ -performance (μ_p) and friction fluctuation ($\mu_{max}-\mu_{min}$), (b) Stability (α) and variability (γ) coefficient.	100
Figure 3A.8. Wear behaviour of the friction composites (a) volumetric wear (%), (b) TGA of the surface ingredients before the tribological test (c) TGA of the ingredients after the tribological test.	102

Figure 3A.9. Worn surface morphology of the friction composites (a, a', and a'') C0, (b, b', and b'') CH, (c, c', and c'') CM, and (d, d', and d'') CW friction composites analyzed with SEM, optical profilometer, and Lorentzian curve fitting of deconvoluted Raman spectroscopy....	104
Figure 3A.10. EDX analysis of the friction composites	106
Figure 3A.11. Wear debris analysis (a) XRD analysis, (b) HR-TEM image, and (c) diffraction pattern.	107
Figure 3B.1. Morphological contrast and elemental mapping of the fabricated friction composites.....	112
Figure 3B.2. The morphology of (a) halloysite, (b) montmorillonite, (c) wollastonite type clay-silicates; (d) derivative thermogravimetric plot, and (e) X-ray diffraction pattern of the clay-type silicates.....	112
Figure 3B.3. Variation in loss modulus as a function of temperature.	114
Figure 3B.4. Friction evolution characteristic and force-displacement behaviour of (a) and (a') C0, (b) and (b') C1, (c) and (c') CH1, (d) and (d') CM1, (e) and (e') CW1.....	115
Figure 3B.5. Comparative friction performance during (a) First fade run (FFR), (b) Second fade run (SFR), (c) First recovery run (FRR), (d) Second recovery run (SRR).	118
Figure 3B.6. Friction performance attribute of the friction composites (a) μ - performance (μ_p) and friction fluctuation ($\mu_{max}-\mu_{min}$), (b) Stability (α) and variability (γ) coefficient.	121
Figure 3B.7. The wear behaviour of friction composites (a) volumetric wear (%), (b) TGA of the composite sliding surface before braking, (c) TGA of the composite sliding surface after braking.	123
Figure 3B.8. Worn surface morphology of (a, a', and a'') C0, (b, b', and b'') C1, (c, c', and c'') CH1, (d, d', and d'') CM1, (e, e', and e'') CW1 friction composites analyzed through SEM, optical profilometry, and Lorentzian curve fit for deconvoluted Raman spectroscopy.	124
Figure 3B.9. The instantaneous braking performance of the friction composites (a) cycle 1, and (b) cycle 5.	128
Figure 3B.10. Schematic of clay type silicate/ MgO assisted contact dynamics under instantaneous braking condition.	129
Figure 4A.1. Variation of storage modulus in clay-based friction composites in terms of temperature for (a) series 1, (b) series 2, and (c) series 3 friction composite	134
Figure 4A.2. Variation of loss tangent in clay-based friction composites in terms of temperature for (a) series 1, (b) series 2, and (c) series 3 friction composite.....	135
Figure 4A.3. Different phases of friction response as a function of speed for clay-based friction composites, (a) series 1, (b) series 2, and (c) series 3	138

Figure 4A.4. Schematic representation of dynamically forming asperity weld joints.....	139
Figure 4A.5. Time dependent Friction response of a clay-based friction composite during (a) stiction, (b) stick-slip and (c) mixed oscillation regimes under different speed	140
Figure 4A.6. Stiction, stick-slip and mixed oscillation period of (a) series 1, (b) series 2 and (c) series 3 friction composites.....	141
Figure 4A.7. Friction response at stiction, stick-slip and mixed oscillation phase (a) average friction coefficient and (b) $\Delta\mu$	143
Figure 4A.8. Electron micrographs of the worn surfaces after stick-slip evaluation for (a) C0, (b) C1, (c) CH, (d) CH1, (e) CM, (f) CM1, (g) CW, and (h) CW1 friction composite.	145
Figure 4A.9. Worn surfaces with colour contrasts represent the various zones on the friction surface based on their hardness for (a) C0, (b) C1, (c) CH, (d) CH1, (e) CM, (f) CM1, (g) CW, and (h) CW1 friction composite. The threshold-images were divided in to three color categories i.e., hard area (light contrast depicted with green), soft area (dark contrast depicted with blue) and moderately hard area (mixed portion depicted with grey)	148
Figure 4A.10. EDX spectra of the worn surfaces after stick-slip analysis for (a) C0, (b) C1, (c) CH, (d) CH1, (e) CM, (f) CM1, (g) CW, and (h) CW1 friction composite.....	150
Figure 4A.11. Fe content of the worn surface of the composites as a measure of transient weld joint formation and relative abrasiveness.	150
Figure 4A.12. Negative slope of coefficient of friction vs. velocity graph during stick-slip [348].....	152
Figure 4A.13. Damped vibration model associated with negative damping behaviour [349, 350]	153
Figure 4A.14. Tornado plot portraying relative importance of the parameters over stick-slip (A_{amp}) amplitude.	157
Figure 4B.1. Evaluation of friction oscillation amplitude (A_{amp})	161
Figure 4B.2. S/N ratio (confirming to lower the better frictional amplitude) at three different levels of control factors i.e., load (A), speed (B), and temperature (C) for (a) Series 1, (b) Series 2, and (c) Series 3 friction composite.	164
Figure 4B.3. Percentage contribution of the control factors (load, speed, and temperature) in friction oscillation	165
Figure 4B.4. The friction oscillation amplitude at (a) experimental event when A_{amp} is maximum (Experiment 4), and (b) at optimized condition.....	165
Figure 4B.5. Scanning electron micrographs of (a) C0, (b) C1, (c) CH, (d) CH1, (e) CM, (f) CM1, (g) CW, and (h) CW1 friction composite.	168

Figure 4B.6. Cumulative braking induced surface topography of the composites post completion of the braking performance evaluation (a) C0, (b) C1, (c) CH, (d) CH1, (e) CM, (f) CM1, (g) CW, and (h) CW1.	171
Figure 4B.7. Cross sectional micrographs of the worn surface with the contrast dependent distribution of Fe and C (as shown in the inset) for (a) C0, (b) C1, (c) CH, (d) CH1, (e) CM, (f) CM1, (g) CW, and (h) CW1 friction composite.	173
Figure 4B.8. Extent of Fe (wt. %) over the worn surface at characteristic locations on the worn surfaces i.e. A- contact patches and B- sporadically scattered wear debris for the friction composites: (a) C0, (b) C1, (c) CH, (d) CH1, (e) CM, (f) CM1, (g) CW, and (h) CW1 (other elements correspond to C, O, Al, Ba, Cu, Si, and Mg).	175
Figure 4B.9. Extent of Fe (wt. %) in wear debris remains inversely proportional to the maximum A_{amp} for the friction composites with various fillers; (a) Halloysite, (b) Montmorillonite, and (c) Wollastonite.	176
Figure 4B.10. Performance hierarchy of the friction composites as per TOPSIS and TOPKOR method.	182
Figure 5.1. Friction response of the composites under cyclic loading for (a) C0, (b) C1, (c) CH, (d) CH1, (e) CM, (f) CM1, (g) CW and (h) CW1.	187
Figure 5.2. Average friction coefficient during the loading and unloading cycle.	190
Figure 5.3. Worn surface morphology of the composites at lower magnification (150X), (a) C0, (b) C1, (c) CH, (d) CH1, (e) CM, (f) CM1, (g) CW and (h) CW1	192
Figure 5.4. Worn surface morphology of the composites at higher magnification (500X), (a) C0, (b) C1, (c) CH, (d) CH1, (e) CM, (f) CM1, (g) CW and (h) CW1.	193
Figure 5.5. Wear behaviour of the composites	195
Figure 5.6. Schematic of fatigue wear mechanism due to cyclic loading.	195
Figure 5.7. Worn surface profile with roughness parameters of the composites (a) C0, (b) C1, (c) CH, (d) CH1, (e) CM, (f) CM1, (g) CW and (h) CW1.	197
Figure 6A.1. Transmission electron microscopy confirming the different morphology of the clay reinforcements (a) tubular shape halloysite, (b) stacked platelet type montmorillonite, and (c) acicular wollastonite.	202
Figure 6A.2. Comparative friction evaluation performance of the CFMs in fade and recovery cycles as per the standard SAEJ661.	212
Figure 6A.3. Friction evolution characteristics of the CFMs: (a) FH, (b) FM, (c) FW under design ideology 1, and (a') MH, (b') MM, and (c') MW under design ideology 2.	213

Figure 6A.4. Thermo-gravimetric plot of worn surface as per design ideology 1 (a) pre-braking condition, (a') after first fade cycle, and design ideology 2 (b) pre-braking condition, (b') after first fade cycle.....	214
Figure 6A.5. friction performance ($\mu_{\text{performance}}$) and friction fluctuation ($\mu_{\text{max}}-\mu_{\text{min}}$) of the clay based CFMs.	215
Figure 6A.6. Stability (α) and variability (γ) coefficients of the CFMs.	216
Figure 6A.7. Friction-fade and friction recovery behaviour of the CFM	217
Figure 6A.8. Volumetric wear of the CFMs as per the design ideology 1 and 2	218
Figure 6A.9. Worn surface morphology of the CFMs after sliding: (a) FH, (b) FM, and (c) FW; (a') MH, (b')MM, and (C') MW.....	219
Figure 6A.10. The volumetric wear (%) of the CFMs considered as primary data set	220
Figure 6B.1. Morphological attributes of the natural silicates (a) tubular halloysite, (b) platy montmorillonite, and (c) acicular wollastonite.	223
Figure 6B.2. Compressive properties of (a and a') natural silicate based CFMs, (b and b') natural silicate- MgO based CFMs.	224
Figure 6B.3. Dynamic mechanical response of the CFMs (a and a') storage modulus, (b and b') loss modulus, and (c and c') loss tangent.....	226
Figure 6B.4. Sensitivity of CoF towards load (a and a'), speed (b and b'), and temperature (c and c').	229
Figure 6B.5. Sensitivity of specific wear rate towards load (a and a'), speed (b and b'), and temperature (c and c').	232
Figure 6B.6. Schematic representation of sliding induced interfacial role of the clay type mineral silicates.	233
Figure 6B.7. Cumulative worn surface morphology of CFMs after load, speed, temperature sensitivity analysis, (a) C0, (b) C1, (c) CH, (d) CH1, (e) CM, (f) CM1, (g) CW, and (h) CW1.	234
Figure 6B.8. Optical-microscopy images of the collected tribo-layers, (a) C0, (b) C1, (c) CH, (d) CH1, (e) CM, (f) CM1, (g) CW, and (h) CW1.	236
Figure 6B.9. Contrast dependent elemental mapping of the collected tribo-layers, (a) C0, (b) C1, (c) CH, (d) CH1, (e) CM, (f) CM1, (g) CW, and (h) CW1.....	237
Figure 6B.10. Raman spectra of the tribo-layer (a) natural silicate based FMs, (b) natural silicate – MgO based FMs.	238
Figure 6B.11. Regression model of the friction force and specific wear rate under (a-a') load sensitivity, (b-b') speed sensitivity, (c-c') temperature sensitivity, results of GD – ANN model	

(d) during training and testing (e) during cross validation of CoF with independent data, and
(f) during cross validation of specific wear rate with independent data.242

LIST OF TABLES

Table 1.1. Worldwide abundance of microplastics in air soil and water	17
Table 1.2. Elemental composition of NAO type and low metallic brake pads [95]	21
Table 1.3. Recent approaches to reduce BWPs via developing wear resistant brake friction composites.....	22
Table 1.4. Recent development in Cu-free brake friction composites.....	27
Table 1.5. Thermal stability of biobased benzoxazine resin binder	33
Table 1.6. Thermal stability of biofibers	36
Table 1.7. Literature review on the bio-fiber addition on brake friction composites	36
Table 1.8. Role of the bio-based friction additives in friction composites	43
Table 1.9. Impacts caused by the disc brakes in seventeen impact categories [246].	46
Table 1.10. Brake friction composites with most desirable functional attributes.....	53
Table 2.1: Average particle size and average fiber diameter of the materials present in friction master batch.	67
Table 2.2. Composition and designation of the composites	68
Table 2.3. Testing schedule according to SAEJ661 standard.....	71
Table 2.4. Steps involved for stick-slip assessment.....	72
Table 2.5. Various levels of control factors	74
Table 2.6. Experimental Design in Taguchi L-9 Orthogonal Array	75
Table 2.7. Experimental design for sensitivity analysis	77
Table 2.8. The learning algorithms with brief description used to train the GD-ANN	81
Table 3A.1. Thermal and physical properties of the clay-type silicates	89
Table 3A.2. Physical and mechanical properties of the composites.....	90
Table 3A.3. Modulus of friction composites	95
Table 3A.4. Friction fade and recovery characteristics of the composites	97
Table 3A.5. The spectral analysis of the D-band and G- band of Raman spectroscopy	105
Table 3A.6. Elemental composition of the worn surfaces	106
Table 3B.1. Modulus of friction composites	114
Table 3B.2. Friction fade and recovery characteristics of the friction composites.....	120
Table 3B.3. The peak intensity ratio of D-band and G-band in Raman spectra of the worn surfaces	127
Table 3B.4. Elemental composition of the worn surface after instantaneous braking performance test.....	129

Table 4A.1. Percentage of the integrated area based on the colour difference over the worn surface of the composites.....	148
Table 4A.2. Attributes associated with stick-slip behaviour	154
Table 4A.3. Stick-slip amplitude (A_{amp}) of the friction composite.....	155
Table 4B.1. Friction oscillation Amplitude $\times 10^{-3}$ (A_{amp}) in Taguchi's L9 OA	162
Table 4B.2: Friction Performance (μ_{avg}) and wear	162
Table 4B.3. Results of the confirmation experiment	166
Table 4B.4. Morphology of natural silicate minerals/ Clay and Maximum $A_{amp} \times 10^{-3}$ in friction composites during Taguchi L-9 experiments.....	169
Table 4B.5: The regression coefficients for the three series of composite friction material .	178
Table 5.1. Friction hysteresis loss of the composites.....	190
Table 6A.1. Composition of clay-based friction composites for primary data set evaluation ^{27,} ²⁸	202
Table 6A.2. Description of the tribological performance attributes (TPAs)	203
Table 6A.3. Magnitude of the TPAs evaluated as per the standard- SAEJ661	204
Table 6A.4. The value of regression coefficients for halloysite, montmorillonite, and wollastonite type clay-based systems.	205
Table 6A.5. Solution properties of optimized composites by solving non-linear optimization for the two set of design ideologies.	207
Table 6A.6. Relative hardness of the clays.....	209
Table 6A.7. Theoretical and real time performance of the CFMs	209
Table 6B.1. The reinforcement effectiveness of the fillers in the CFMs.....	225
Table 6B.2. Elemental composition of the tribo-layers	238
Table 6B.3. The peak intensity ratio of G-band and D-band in Raman spectra of tribo-layer	239
Table 6B.4. Regression coefficients for the friction force and specific wear rate.....	241
Table 6B.5. Hyper parameter optimization of the GD-ANN model.....	244
Table 6B.6. The sequential splitting of the dataset for training and testing of the GD- ANN model.....	245
Table 6B.7. Weightage to layer 1 from the input	245
Table 6B.8. Weightage to layer 2 from layer 1.....	246
Table 6B.9. Weightage to layer 3 from layer 2.....	246
Table 6B.10. Bias in GD - ANN Model	247
Table 6B.11. The comparison between regression models and GD-ANN model.....	247

LIST OF ABBREVIATIONS

μ

μ - instantaneous: μ_i , 66

μ -performance: μ_p , 92

A

Aluminum: Al, 21

Aluminum oxide: Al_2O_3 , 38

Amplitude of creep groan: $\Delta\mu$, 146

Analytical hierarchy process- technique for order performance by similarity to ideal solution: AHP-TOPSIS, 52

Applied load: L, 169

Artificial Neural Network: ANN, 54

Average friction coefficient: μ_{avg} , 153

Average surface roughness: R_a , 95

B

Barium: Ba, 21

Barium sulfate: $BaSO_4$, 39

Binder: B_n , 49

Brake wear debris: BWDs, 19

Brake wear dust: BWD, 4

C

Calcium: Ca, 21

Calcium carbonate: $CaCO_3$, 39

Carbon: C, 165

Cashew shell nut liquid: CSNL, 26

Closeness coefficient: CC_i , 174

Coefficient of determination: R^2 , 199

CoF: μ , 71

Complex proportional assessment: COPRAS, 52

Composite friction materials: CFMs, 59

Copper: Cu, 21

Criteria importance through inter-criteria correlation: CRITIC, 52

Critical speed: V_c , 148

D

Damping parameter: $\tan \delta$, 126

Derivative thermogravimetric analysis: DTGA, 105

Design of experiments: DOE, 53

Desirable: D, 49

Disc temperature rise: DTR, 66

Dynamic mechanical analysis: DMA, 72

E

Electric vehicles: EVs, 19

Elimination and Choice Expressing Reality: ELECTRE, 52

Energy-dispersive X-ray spectroscopy: EDX, 28

F

Fiber: F_b , 49

Field emission scanning electron microscopy: FESEM, 73

Filler: F_l , 49

First fade run: FFR, 64

First recovery run: FRR, 64

Fraction of hard contact phase: A_h , 148

Friction assessment testing rig: FCTR, 56

Friction fade %: FF %, 197

Friction fluctuation: $\mu_{\max} - \mu_{\min}$, 92

Friction modifier: F_m , 49

friction oscillation amplitude: A_{amp} , v

Friction recovery %: FR %, 197

Full-width half maxima: FWHM, 95

G

Glass transition temperature: T_g , 83

Gradient descent with momentum term and adaptive learning rate: GDX, 74

Gradient descent: GD, 74

Gradient descent algorithm adaptive learning rate back-propagation: GDA, 74

gradient descent learning algorithm based-artificial neural network: GD-ANN, vii

H

Halloysite: HNT, 62

High-resolution transmission electron microscopy: HRTEM, 72

I

Intensity of disordered peak: I_D , 95

Intensity of graphitized peak: I_G , 95

International Agency for Research on Cancer: IARC, 28

Iron: Fe, 21, 165

L

Life cycle assessment: LCA, 45

Load: L, 148

Loss modulus: E'' , 72

M

Magnesium: Mg, 21, 121

magnesium oxide: (MgO), iii

Metal disulfides: Dichalcogenides, 37

Micro-orifice uniform deposit impactors: MOUDI, 18

Montmorillonite: MMT, 62

Movable cellular automata: MCA, 52

Multi-criteria decision making: MCDM, 39

Multi-objective optimization based on ratio analysis: MOORA, 52

Multiple attribute decision making: MADM, 39

Multiplicative exponent weighting: MEW, 52

Multiwalled carbon nanotube: MWCNT, 52

N

Negative Euclidean distance: S_i^- , 173

New York State: AB 10871, 24

Noise vibration harshness: NVH, 7

Non-asbestos organic: NAO, 6

Non-asbestos organic brake in east central Europe: NAO-ECE, 19

O

One variable at a time: OVAT, 70

Orthogonal array: OA, 68

P

Particulate matter: PM, 2

Percentage friction hysteresis loss: %FHL,
70

Performance index: P_i , 173

Phenol-formaldehyde: PF, 31

Positive Euclidean distance: S_i^+ , 173

Potassium: K, 21

Potassium titanate: $K_2Ti_6O_{13}$, 38; $KTiO_2$,
30

Powell

Beale conjugate gradient algorithm:
CGB, 74

Promaxon-D: $Ca_6Si_6O_{17}(OH)_2$, 29

R

Regret index: R_i , 174

Reinforcement effectiveness: r , 217

Response surface methodology: RSM, 53

Rhode Island House: HB 7997, 24

Root mean square error: RMSE, 55

Root mean square surface roughness: R_q ,
95

S

scanning electron microscopy–energy-
dispersive X-ray spectroscopy: SEM–
EDX, iv

Second fade run: SFR, 64

Second recovery run: SRR, 64

Signal to noise ratio: S/N ratio, 68

Silicon carbide: SiC, 38

Silicone: Si, 21

Sliding velocity: V , 169

Stability coefficient: α , 92

Stiffness: k , 147

Strength-weakness-opportunity-threat:
SWOT, 42

Sulphur: S, 21

Suspended airborne particulate matter:
SPM, 3

T

Targeted material design: TMD, 194

technique for an order of preference by
similarity to ideal solution: TOPSIS, v

Temperature: T , 106, 170

thermogravimetric analysis: TGA, 72

Third body abrasion: TBA, 39

Tin: Sn, 21

Tin disulfide: SnS_2 , 26

Titanium: Ti, 21

Tribological performance attributes: TPAs,
197

Tungsten disulfide: WS_2 , 26

Tyre wear debris: TWD, 19

U

Undesirable: UD, 49

V

Variability coefficient: γ , 92

W

Wear volume %: WV %, 197

Weightage: W_i , 172

Wollastonite: WST, 62

X

X-ray diffraction: XRD, 72

Z

Zinc: Zn, 21

Zircon: ZrSO₄, 38

Zirconium oxide: ZrO₂, 38

M

μ -level during stiction: μ_{stiction} , 145